TECHNICAL NOTE:

HOMOGENIZATION OPTICS TO IMPROVE DETECTABILITY OF FLUORESCENCE RESPONSE TO A SINGLE LASER PULSE: DETECTION OF FECES ON APPLES

P. Shilts, P. Motabar, A. M. Lefcourt, M. S. Kim, U. Tasch

ABSTRACT. *Fecal contamination of produce in fields is a known food safety risk. It is theoretically possible to enhance the current practice of visually inspecting fields for fecal material prior to harvest by using imaging to detect the fluorescence response of fecal material to UV excitation. For field application, an expanded-beam pulsed laser and a gated-intensified camera can be used for imaging to negate problems due to reflected ambient light masking fluorescent responses. A particular problem when using an expanded laser beam for illumination is that temporally inconsistent and spatially non-uniform energy distributions can produce false positives. This technical note describes an optical system that expands and homogenizes a high-energy laser beam using a lightpipe. To validate the homogenizing optics, images were acquired using both homogenizing optics and a simple optics system that did not incorporate a lightpipe. Sequential images acquired using uniform fluorescent targets demonstrated that temporal variability in illumination intensity for individual pixels was reduced when using the homogenizing optics. For single images, the Gaussian energy distribution seen when using simple optics was eliminated when using the homogenizing optics. To test how these technical advantages might affect the quality of acquired images in practice, apples artificially contaminated with cow feces were imaged using a multispectral adapter with 678 and 500 nm filters. Threshold detection rates for 1:1000 dilutions were 50% and 15% when using the homogenizing and simple optics, respectively. In addition, for 1:2 and 1:20 dilutions using 678/500 nm ratio images, the relative magnitude of the measured response was greater when using the homogenizing optics. It is recommended that homogenizing optics be used to expand pulsed laser beams that are used to excite fluorescence responses.*

Keywords. *Fecal detection, Fluorescence imaging, Food safety, Lightpipe, Machine vision, Time-resolved imaging.*

There are nearly 50 million cases of foodborne illnesses in the U.S. each year, resulting in 130,000 hospitalizations and over 3,000 deaths (CDC, 2011), and leafy green produce accounts for 23% of all foodborne illnesses (Painter et al., 2013). To reduce risks associated with leafy greens, produce fields are visually surveyed for fecal material immediately prior to harvest (CALGMA, 2013). To enhance this visual observation practice, an imaging system to detect fecal contamination in produce fields is under development in our laboratory. The system uses an expanded-beam pulsed laser for illumination. Problems with the quality of illumination resulted in the development of the homogenizing expansion optics described herein.

Imaging has become a useful tool for evaluating agricultural commodities (Kim et al., 2005; Sun, 2010; Zhang et al., 2012). For example, fluorescence responses to UV excitation have been used to detect fecal contamination on apples (Kim et al., 2002; Lefcourt et al., 2003) and aflatoxin contamination on hazelnuts (Kalkan et al., 2011). A time-resolved (ns) multispectral imaging system using a pulsed laser for fluorescence excitation was previously developed to allow examination of fluorescence decay characteristics and to allow potential use of the system under outside ambient lighting conditions (Kim et al., 2008; Lefcourt et al., 2003, 2005a). Generally, reflected ambient light masks most fluorescence responses due to the relative differences in intensity. However, the effective megawatt power of an expanded laser beam results in short-term (ns) fluorescence responses that are orders of magnitude brighter than reflected ambient sunlight. The major problems with the expanded laser illumination used in the prior studies were lack of temporal consistency and spatial homogeneity.

Each laser pulse generally incorporates a number of random effects. In laboratory experiments, this variation is dealt with by averaging the responses to a selected number of excitation pulses (Kim et al., 2008; Lefcourt et al., 2005a). Even with averaging, the illumination intensity across the imaging field may not be uniform, i.e., the intrinsic energy distribution profile of a laser beam is not uniform, with the most common spatial distribution being Gaussian (Dickey and Holswade, 2000). However, if the illumination intensity at a given pixel location is consistent

Submitted for review in September 2013 as manuscript number FPE 10443; approved as a Technical Note for publication by the Food & Process Engineering Institute of ASABE in March 2014.

Mention of company or trade names is for description only and does not imply endorsement by the USDA. The USDA is an equal opportunity provider and employer.

The authors are **Patrick Shilts,** Graduate Student, **Payam Motabar,** Graduate Student, **Alan M. Lefcourt,** Biomedical Engineer, and **Moon S. Kim,** Physicist, USDA-ARS Environmental Microbial and Food Safety Laboratory, Beltsville, Maryland; **Uri Tasch,** Professor, Department of Mechanical Engineering, University of Maryland, Baltimore County, Baltimore, Maryland. **Corresponding author:** Alan M. Lefcourt, Rm 21, Bldg 303, BARC-East, Powder Mill Rd., Beltsville, MD 20705; phone: 301-504-8450, ext. 258; e-mail: alan.lefcourt@ars.usda.gov.

over time, it is often possible to derive a spatial normalization function. It is also possible to correct for uneven spatial illumination by taking the ratio of simultaneous measurements made at two different wavelengths on a pixel-by-pixel basis (Kim et al., 2002; Lefcourt et al., 2006). In field situations, the ability to average responses acquired over time may not exist. For example, to survey production fields, the imaging system could be mounted on a vehicle and driven through the field, with each acquired image corresponding to a new field location.

This study describes an optical system that expands and homogenizes a high-energy laser beam using a lightpipe. The benefit of the homogenizing optics is evaluated by comparing images of different targets illuminated using either the homogenizing optics or a similar expansion optics configuration that did not incorporate a lightpipe. The ultimate goal is to develop a sensitive fluorescence detection system that uses only a single homogenized laser pulse for detection.

MATERIALS AND METHODS

LASER AND CAMERA

The illumination source is a pulsed (~6 ns pulse width) Nd:YAG laser (Ultra 100 THG WS MVAT, Quantel USA, Bozeman, Mont.) with a power supply (ICE450) modified by Quantel USA to provide a digital pulse 100 ns prior to the Q-switch trigger (fig. 1). The laser emits a frequency-tripled 355 nm beam with a maximum pulse rate of 20 Hz and a maximum energy of 31.5 mJ per pulse. The laser head includes an attenuation module. The laser beam has a Gaussian profile with a diameter of 3.2 mm and a divergence of 3.4 mrad, as measured by Quantel USA.

Images were acquired using an intensified gated charge-coupled device (CCD) camera (iStar, Andor Technologies, Belfast, Northern Ireland). The camera is thermoelectrically cooled to -20°C. The pixel numbers, size, and bit resolution are 1024 × 1024, 26 × 26 μm, and 16, respectively. The camera has a C-mount connector that was used to attach an *f*2.8/75 mm lens (Computar FA Megapixel, CBC (America) Co., New York, N.Y.) or a multispectral adapter (MSAI-04, Optical Insights, Ariz.) and an *f*1.4/7.5 mm lens (Rainbow CCTV, International Space Optics SA, Irvine, Cal.). The multispectral adapter divides the CCD into four identical regions and allows the use of a different interference filter for each region (fig. 2). The filters used in this study were 25 nm FWHM (full width at half maximum) at 500 nm, 10 nm FWHM at 660 nm, 22 nm FWHM at 678 nm, and 10 nm FWHM at 690 nm (Melles Griot, Albuquerque, N.M.). In order to facilitate acquisition of registered images for the four quadrants, software was created to provide real-time feedback during prism adjustment of the multispectral adapter.

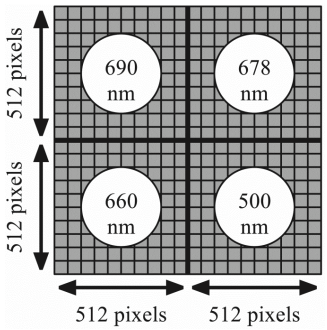

Figure 2. The multispectral adapter divides the CCD into four identical quadrants, with a different interference filter for each quadrant.

Images capture is controlled using software developed in-house using Microsoft Visual Basic (ver. 6, Microsoft Corp., Redmond, Wash.) and an Andor Technologies software development kit. The software sets the gate delay relative to the onset of the laser pulse, gate width, and laser attenuation, and initiates image acquisition. For each image, a single expanded laser pulse was used for illumination. Acquired images were corrected for dark current and saved using tagged image file format (TIFF).

LASER BEAM EXPANSION OPTICS

The homogenizing (H) beam expansion optics use a -50 mm plano-concave (PCV) lens, a 25 mm double-convex (DCX) lens, a hexagonal light pipe (10 mm aperture × 125 mm length; Edmund Optics Inc., Barrington, N.J.), and a 40 mm DCX lens (fig. 3). The lens material is fused silica, and each lens has an anti-reflective UV coating (Edmund Optics Inc. or Thorlabs Inc., Newton, N.J.). To address potential on-axis backscattering, the expansion optics incorporate a 4 mm iris along with a 355 nm laser window tilted 5° from the optical axis (Techspec 1/20λ high-power laser-line window, Edmund Optics Inc.). The optics are

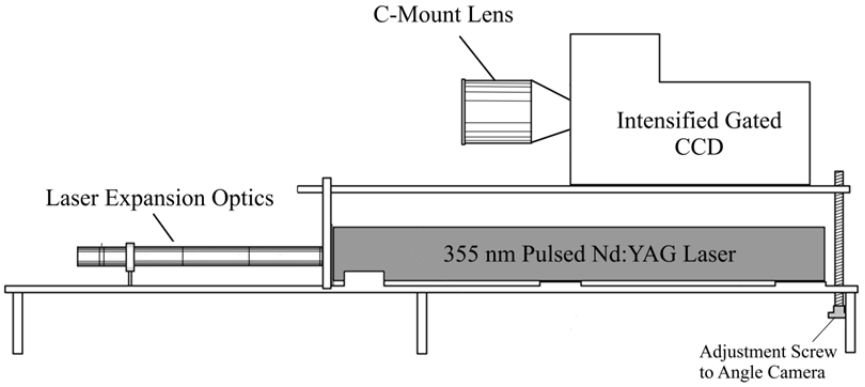

Figure 1. Anodized aluminum mount for camera and laser. When used, the multispectral adapter is placed between the lens and the camera.

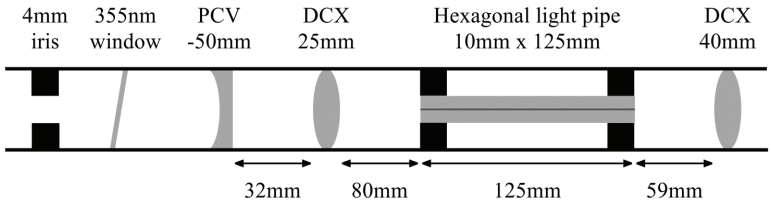

Figure 3. Lens configuration used for homogenizing beam expansion.

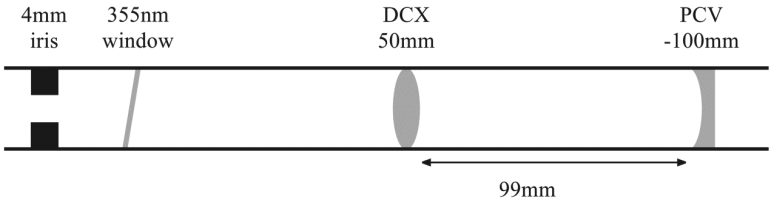

Figure 4. Lens configuration used for simple beam expansion.

mounted in segmented 25.4 cm diameter anodized aluminum lens tubes (Thorlabs Inc.). To allow evaluation of the benefits of using the lightpipe for homogenization, images were also acquired using a similar set of expansion optics minus the lightpipe; the simple (S) beam expansion optics use a 50 mm double convex (DCX) lens and a -100 mm plano-concave (PCV) lens (fig. 4).

Laser Beam Energy Measurement

Power measurements were taken using a power meter (PE25-BB, Ophir Optronics Ltd., Danvers, Mass.) placed 30 cm from the laser aperture. Single measurements were made using both types of expansion optics for a progression of laser attenuations. Transmittance losses were calculated relative to the measured energy of the raw laser beam using the same laser attenuation but no expansion optics.

Experimental Trials

First, 30 sequential images of glossy photo paper (Q1428A, Hewlett-Packard, Palo Alto, Cal.) mounted 133 cm from the front of the laser were acquired using only the lens, a 5 ns gate delay, a 20 ns gate width, a gain of 5, and a laser attenuation of 150 out of 255. Second, using the multispectral adapter, 30 sequential images of the glossy paper and also of red fluorescent paper (Neon Bond, Pacon, Appleton, Wisc.) were acquired as above except using a gain of 100. Finally, five sequential images of eight apples mounted 86 cm from the front of the laser were acquired as above except using a gain of 200. The apples were tree-run Golden Delicious inoculated with 20 µL drops of fresh cow feces at four dilutions made by weight using distilled water: 1:2, 1:20, 1:200, and 1:1000 (fig. 5).

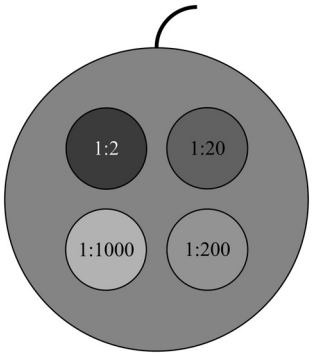

Figure 5. Schematic of placement of manure dilutions on apples.

Data Analysis

Paper Targets

A circular region of interest (ROI) was created that represented about 95% of the area of a response measured using the simple optics for illumination. This ROI was applied to images acquired using both types of expansion optics. Means, standard deviations, and coefficients of variation (CV) were calculated for individual pixels across replicate sequential images; these measures were also calculated across pixels for individual images. Images representing statistical measures were created, and a false-color routine that converts 255-bit gray-scale images into six segments was applied to allow better visualization of the measures. Measures for individual images were plotted sequentially to show the variation in illumination from one laser pulse to another.

To address the bias associated with the inherent energy distribution profile of the laser's Gaussian beam, comparisons were also made after normalization of images. A normalization function was created by taking a subset comprising 10 of the 30 sequentially acquired images, finding mean pixel values across the 10 images, and then scaling and inverting these averages. This normalization function was then applied to the remaining 20 images.

Apples

Individual and 678/500 nm ratio images were analyzed. A semi-automated routine was used to place circular ROIs, 28 pixels in size, over the four contamination sites on each apple. To allow comparison of contaminated and uncontaminated regions on each apple, masks of the uncontaminated areas on each apple were created. First, an intensity threshold was used to separate the apple from the background. Second, the ROIs of the contamination sites were subtracted. Finally, the area of the mask was reduced using a dilation filter. The ROI and apple masks were identical across all images of an individual apple. For each image, the maximum pixel intensity value within each ROI and the

next-to-maximum intensity value for the apple surface remaining after application of the corresponding mask were calculated. The next-to-maximum value for the apple surface was used instead of the maximum value because outliers sometimes occur in ratio images due to sub-pixel differences in image alignment between the 678 and 500 nm images.

The number of contamination spots for each dilution where the maximum intensity value exceeded the maximum apple surface value was determined for each type of laser expansion. Where indicated, differences between ROI and apple maximums were calculated by dilution and laser expansion optics.

Results and Discussion

Laser Beam Energy Profile and Normalization

One aspect of illumination quality is spatial uniformity. To substantiate that the laser beam energy profile was Gaussian and to investigate whether the beam illumination could be normalized, fluorescence responses were imaged using both homogenizing (H) and simple (S) expansion optics. Figure 6 shows images of fluorescence responses of white glossy paper that were captured in response to single laser pulses; the inherent Gaussian distribution of the laser energy is evident for S, while the hexagonal shape of the light pipe is evident for H. The false-color images demonstrate that the S optics produce an illumination profile with a steep gradient in intensity from the center to the edges and that the H optics produce more uniform illumination with a shallow gradient from top to bottom. The shallow gradient is probably the result of imperfect alignment of the expansion optics. The false-color images also demonstrate the effectiveness of post-acquisition normalization, where spatial illumination gradients are essentially eliminated. Results using the multispectral adapter were qualitatively identical; the Gaussian response profile was evident in all cases where the S optics were used for expansion, and in all cases normalization essentially eliminated spatial variability. Due to the similarity of results, the corresponding images using the multispectral adapter are not presented.

Spatial and Temporal Uniformity of Laser Beam Expansions

Temporal consistency of illumination is important in relation to the potential for false positives, e.g., random, relatively bright areas of illumination can produce localized elevated fluorescence responses. A common mechanism used to reduce the impact of these localized responses is to raise the detection threshold, which decreases the sensitivity of the detection method. To examine the temporal consistency of illumination provided by an expanded laser beam, the consistency of illumination intensity of individual pixels over sequential laser pulses can be examined. Figure 7 shows false-color images representing means, standard deviations, and coefficients of variation for a sequence of images of white glossy paper captured using only a lens and either H or S optics for fluorescence excitation. The images in figure 6 were included in the sequence of images used to calculate the results shown in figure 7. For raw image sequences, the mean intensities for H are essentially uniform compared to S. Normalization resulted in nearly uniform mean intensities for both H and S; however, the effects of the sharp drop in intensity at the edges of S illumination can still be seen. The CV images demonstrate the advantage of the H expansion optics in terms of consistency of illumination intensity of individual pixels. For H, the CV values are consistently low. For S, the CV values for individual pixels across sequential images are not spatially uniform; areas with higher CV include small areas located toward the center of illumination, and the non-uniformity remains after normalization. Areas of relatively high CV

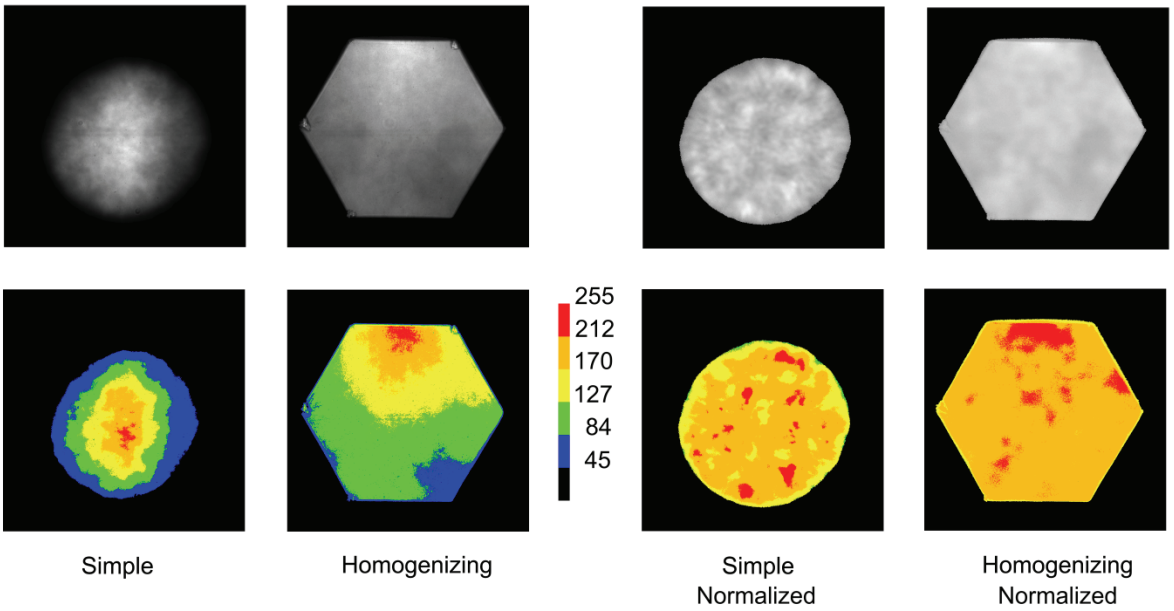

Figure 6. Representative images of fluorescence responses acquired using only a lens with simple or homogenizing expansion optics with and without post-acquisition normalization, and corresponding false-color images.

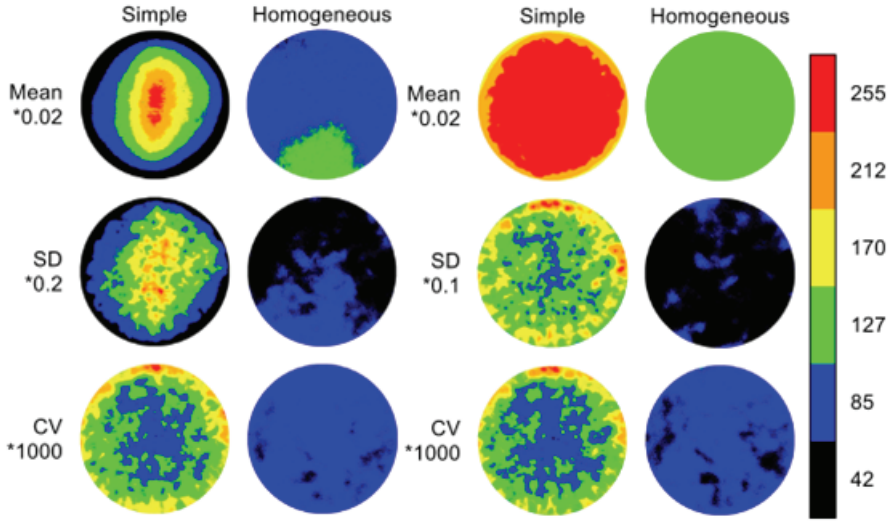

Figure 7. False-color representations of means, standard deviations (SD), and coefficients of variation (CV) calculated for individual pixels across sequences of images acquired using only a lens with simple or homogenizing expansion optics without (left, $n = 30$) and with (right, $n = 20$) post-acquisition normalization. The target is white glossy photo paper. Ten images were used to create normalization functions.

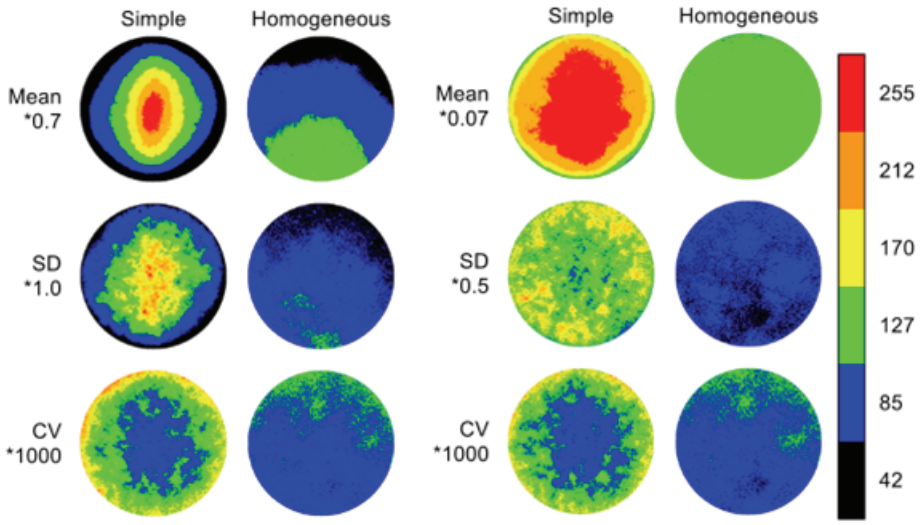

Figure 8. False-color representations of means, standard deviations (SD), and coefficients of variation (CV) calculated for individual pixels across sequences of images acquired using a multispectral adapter and 678 nm filter with simple or homogenizing expansion optics without (left, $n = 30$) and with (right, $n = 20$) post-acquisition normalization. The target is red fluorescent paper. Ten images were used to create normalization functions.

have the greatest potential for generating false positives, and even one small area within the region used to illuminate a target can be problematic.

Figure 8 is similar to figure 7 except that it shows false-color images representing statistics when using the multispectral adapter and the 678 nm filter. Results for the multispectral adapter are directly comparable to results for the lens alone, and results for the 678 nm filter are comparable to results for the other three filters (not shown). Again, the CV images demonstrate the advantage of the H optics in terms of consistency of illumination intensity of individual pixels over time.

Figure 9 shows averaged CV values of intensities across individual images as a function of image number. The CV values for S prior to normalization ranged from 0.6 to 0.7 using either a lens alone or a lens with the multispectral adapter and the 678 nm filter. Comparable CV values for H ranged from 0.2 to 0.3 when using the lens alone and from 0.3 to 0.4 when using the 678 nm filter. Normalization reduced CV values for both S and H, but CV values for H were still roughly half those for S. The results were similar when using the multispectral adapter and any of the other interference filters.

Laser Beam Energy Loss

The purpose for measuring energy loses for the H and S expansion optics was to determine if the loss due to homogenization might be excessive. In reality, it is hard to relate the measured losses to use of the optics in a real-world application. For example, if the goal was to measure fluorescence responses in a produce field, adequate illumination for detection would have to be provided to the far corners of the rectangular region being imaged. For the H optics, the rectangular area could be as wide as the actual

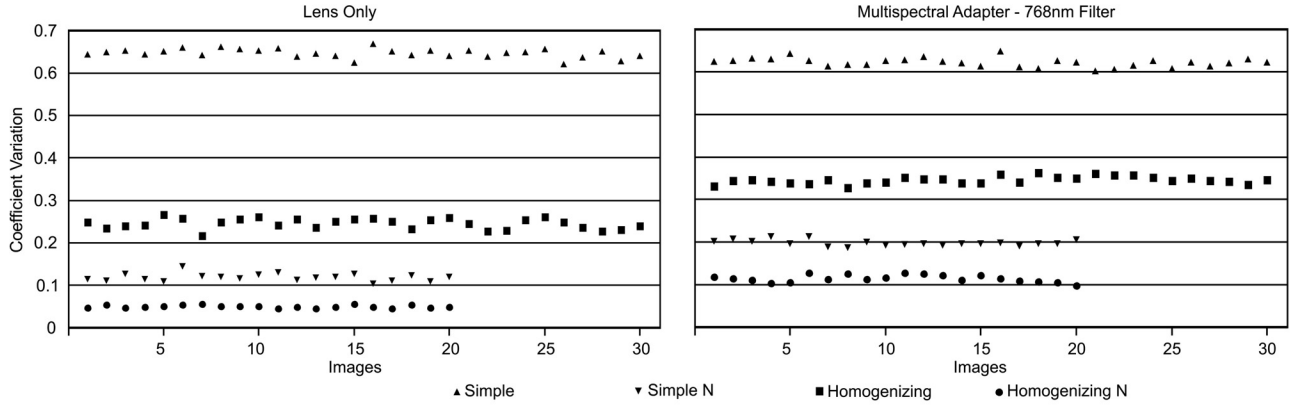

Figure 9. Coefficients of variation (CV) across pixels by image for the sequences of images used to generate figures 7 and 8. Normalization (N), which resulted in an image count of 20 as 10 images were used to construct the normalization functions, reduced the CV; however, the variability when using homogenizing optics was consistently lower than when using simple optics.

Table 1. Energy measurements when using no, simple, and homogenizing expansion optics and relative energy losses compared to using no expansion optics at six laser attenuation levels.

	Energy (mJ)			Energy Loss (%)	
Attenuation	No	Simple	Homo.	Simple	Homo.
30/255	0.56	0.55	0.49	1.8	12.5
40/255	1.05	1.02	0.91	2.9	13.3
50/255	1.70	1.66	1.49	2.4	12.4
60/255	2.48	2.43	2.19	2.0	11.7
70/255	3.28	3.19	2.88	2.7	12.2
80/255	4.22	4.13	3.74	2.1	11.4
Average				2.3	12.2

illumination field; however, for S optics, the rectangular area would have to be less than the maximum area that could be inscribed in the circular illumination area, as energy near the outer edges of the S illumination profile would be very low due to the Gaussian profile of the illumination.

Energy measurements recorded for single-shot laser pulses for no, S, and H expansion optics at six energy attenuation levels are shown in table 1. Compared to using no expansion optics, the average energy losses for S and H optics were 2.3% and 12.2%, respectively. These results indicate that the energy losses due to homogenization are not excessive.

TESTS WITH CONTAMINATED APPLES

The tests with paper targets demonstrated the technical advantages of the homogenizing expansion optics in comparison to the simple expansion optics. To examine how these technical advantages might affect the quality of acquired images in practice, tests were conducted on apples artificially contaminated with cow feces. Contaminated apples were selected as targets because of laboratory experience with using laser-induced fluorescence to detect feces on apples (Kim et al., 2008; Lefcourt et al., 2003, 2005a, 2005b) and correspondence with the problem of detecting feces in produce fields. A particular problem for detecting fecal material in fields is that the fluorescence responses of feces are very similar to the responses of intact plants, with both due to chlorophyll-related compounds in plant materials. For feces, the digestion of plant materials creates breakdown products that shift the peak wavelength of the primary fluorescence response curve. The response peak for feces from most animals is around 675 nm (Kim et al., 2003), while the peak for plants is around 685 nm (Chappelle et al., 1991; Murata et al., 1966). As there is broad overlap between the response regions, a random event causing a relative increase in illumination intensity for a small area on a plant surface could result in a fluorescence response that could easily be misinterpreted as fecal material. Digestion also results in a lengthening of the fluorescence decay time (Lefcourt et al., 2005a; Tewey, 2013).

Selection of the filters used in the multispectral adapter was influenced by the known difference in response peaks for fecal and plant materials. The 660 and 690 nm filters were selected to see if this difference could be used to provide a basis for detection, e.g., by creating difference images using these filter images. Preliminary tests indicated that 678 nm images alone led to better detection results, and 660 and 690 nm images were not subject to further analyses.

The simplest method that can be used for detection of the applied feces is to use a threshold to separate contaminated areas from normal apple surfaces in images. A number of techniques can be used to increase the sensitivity and selectivity of detection, generally by using a function that incorporates information from a number of adjacent pixels. As the goal of the apple test was to essentially contrast the quality of the signal produced using the different expansion optics, and enhanced detection techniques would likely mask these differences, all comparisons were made using only thresholds for detection.

However, the normalization procedure used with paper targets is not really appropriate for use in situations where the surface of the target is not flat. When the surface is not flat, parallax can produce significant errors (Tewey, 2013). A common method to deal with uneven illumination is to use ratios of images acquired at two different wavelengths. Assuming that the fluorescence responses at both wavelengths are linearly proportional to the illumination intensity, the calculated ratio at each pixel location will not be a function of illumination intensity, i.e., the illumination intensities in the numerator and denominator will cancel out. Thus, ratios theoretically can compensate for both spatial and temporal non-uniformity in illumination. Ratios of 678 nm fluorescence images to images acquired in the blue region of the spectra, such as at 500 nm, have been demon-

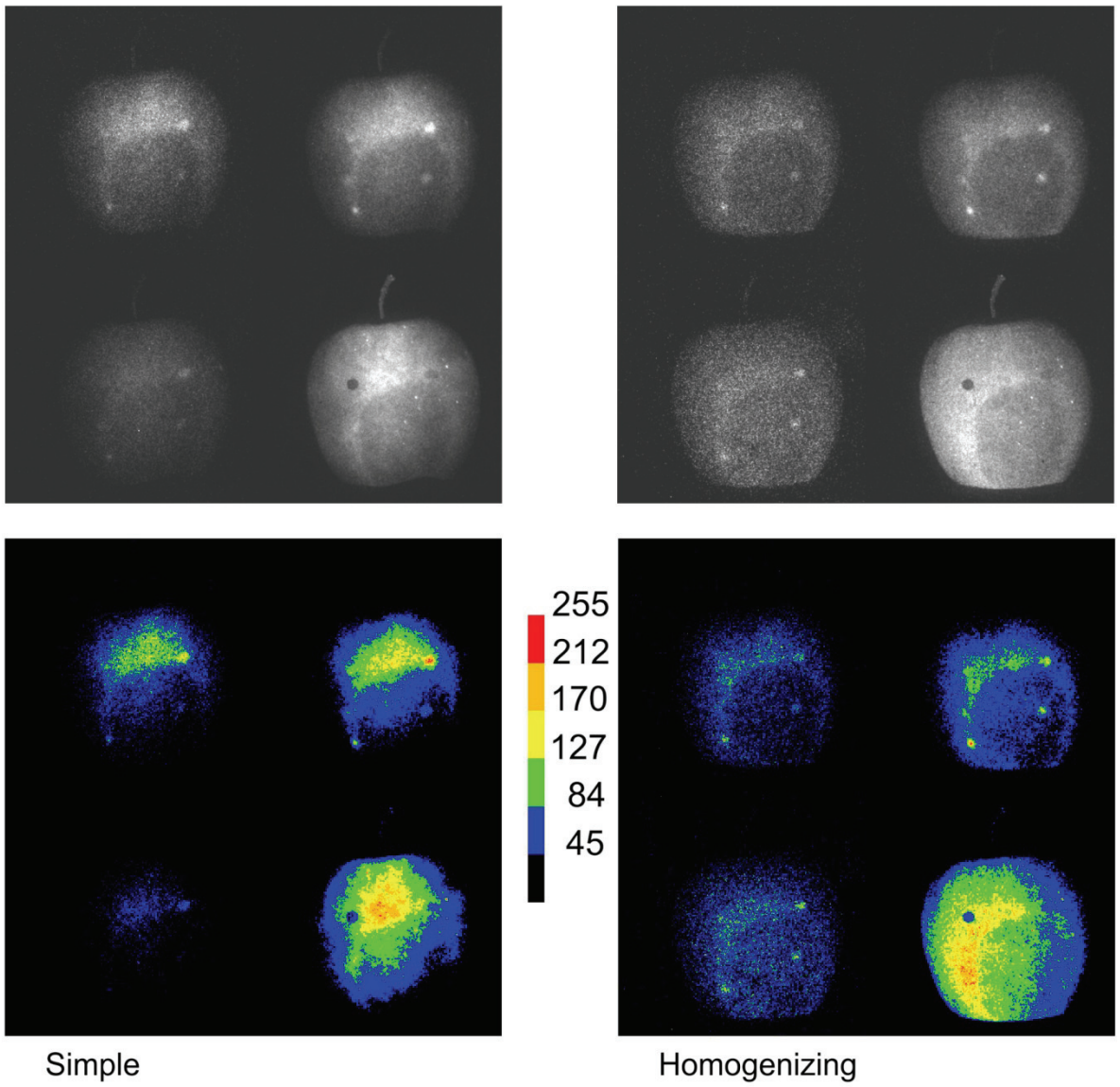

Figure 10. Representative fluorescence responses of manure applied to an apple at 690, 678, 500, and 660 nm (clockwise from upper left, respectively) when using simple or homogenizing optics along with corresponding false-color images.

strated to be advantageous for the detection of feces on apples (Kim et al., 2002; Lefcourt et al., 2006). To examine the impact of the type of expansion optics on detection using ratio images, 678/500 nm ratio images were tested using threshold detection.

Figure 10 shows fluorescence responses for a representative apple. Comparison of the images acquired using H and S optics demonstrates that the H optics reduce the intensity variability across the face of the apples and provide better and more consistent contrast between contamination sites and the surrounding apple surface. Generally, detection rates were similar with three exceptions (table 2). Ratio images improved detection of 1:2 and 1:20 dilutions for both types of expansion optics compared to simple images at 678 nm and allowed detection of all 1:2 and 1:20 contamination sites. This result is consistent with results from previous studies and is due, at least in part, to a complex interaction in which fecal material induces an increase in the fluorescence response of the underlying apple surface and high concentrations of feces quench the response of the underlying apple surface (Lefcourt et al., 2003, 2005c). For 1:200 contamination sites, detection rates were similar when using H optics for both simple and ratio images and when using S optics for ratio images. The detection rate using S optics for simple images was lower. For 1:1000 contamination sites, H optics along with simple images provided superior detection results and allowed detection of more than half of the contamination sites. Detection rates for all other cases were around 15%. The enhanced 1:200

Table 2. Numbers of contamination spots detected for the four applied manure dilutions by expansion optics (simple or homogenizing) and image type (678 nm or 678/500 nm ratio). The number of spots tested for each dilution is 8 apples × 5 repetitions per apple, for a total of 40.

	Applied Manure Dilution			
Treatment	1:2	1:20	1:200	1:1000
Homo. 678 nm	32	38	25	21
Homo. ratio	40	40	25	5
Simple 678 nm	34	29	0	6
Simple ratio	40	40	26	6

Table 3. Average measured differences between the maximums for the contamination sites and corresponding apple surface for ratio images by type of expansion optics (homogenizing or simple).

	Applied Manure Dilution	
Treatment	1:2	1:20
Homo. ratio	66.7	65.7
Simple ratio	58.8	57.8

and 1:1000 detection rates for H optics confirm the superiority of these optics.

Given that detection rates using ratio images were 100% for 1:2 and 1:20 dilutions for both types of expansion optics, actual differences between measurements for contamination sites and apple surfaces were examined to try to better differentiate the relative effectiveness of H and S optics (table 3). The results show that the differences were consistently larger for H optics. The larger differences can be interpreted as H providing increased detection sensitivity when compared to S.

CONCLUSIONS

Tests of pixel-by-pixel illumination variability using uniform paper targets demonstrated the technical superiority of homogenizing expansion optics as compared to simple, non-homogenizing, expansion optics. The homogenizing expansion optics provided illumination with better spatial and temporal consistency. Tests using apples artificially contaminated with dilutions of manure demonstrated that the technical superiority of the homogenizing optics translated into greater sensitivity for detecting fecal contamination sites. The homogenizing optics, along with a simple threshold, allowed detection of about 50% of the 1:1000 dilution sites, in contrast to 15% detection when using the simple optics. For the 1:2 and 1:20 dilutions, when using 678/500 nm ratio images for detection, all contamination sites were detected regardless of the expansion optics used; however, the margin of detection was greater for the homogenizing optics. It is recommended that homogenizing optics be used for expansion of pulsed laser beams used to excite fluorescence responses from targets.

REFERENCES

CALGMA. (2013). Commodity-specific food safety guidelines for the production and harvest of lettuce and leafy greens. Sacramento, Cal.: California Leafy Green Products Handler Marketing. Retrieved from www.caleafygreens.ca.gov/food-safety-practices.

CDC. (2011). CDC estimates of foodborne illness in the United States: Findings. Atlanta, Ga.: Centers for Disease Control and Prevention. Retrieved from www.cdc.gov/foodborneburden/2011-foodborne-estimates.html.

Chappelle, E. W., McMurtrey, J. E., & Kim, M. S. (1991). Identification of the pigment responsible for the blue fluorescence band in the laser-induced fluorescence (LIF) spectra of green plants, and the potential use of this band in remotely estimating rates of photosynthesis. *Remote Sensing Environ., 36*(3), 213-218. http://dx.doi.org/10.1016/0034-4257(91)90058-E.

Dickey, F. M., & Holswade, S. C. (2000). *Laser Beam Shaping: Theory and Techniques.* New York, N.Y.: Marcel Dekker.

Kalkan, H., Beriat, P., Yardimci, Y., & Pearson, T. C. (2011). Detection of contaminated hazelnuts and ground red chili pepper flakes by multispectral imaging. *Computers Electr. Agric., 77*(1), 28-34. http://dx.doi.org/10.1016/j.compag.2011.03.005.

Kim, M. S., Lefcourt, A. M., Chen, Y. R., Kim, I., Chan, D. E., & Chao, K. (2002). Multispectral detection of fecal contamination on apples based on hyperspectral imagery: Part II. Application of hyperspectral fluorescence imaging. *Trans. ASAE, 45*(6), 2039-2047. http://dx.doi.org/10.13031/2013.11416.

Kim, M. S., Lefcourt, A. M., & Chen, Y. R. (2003). Optimal fluorescence excitation and emission bands for detection of fecal contamination. *J. Food Prot., 66*(7), 1198-1207.

Kim, M., Lefcourt, A., & Chen, Y. R. (2005). Multispectral laser-induced fluorescence imaging techniques for nondestructive assessment of postharvest food quality and safety. *Acta Hort., 682*(2), 1379-1385.

Kim, M. S., Cho, B., Lefcourt, A. M., Chen, Y. R., & Kang, S. (2008). Multispectral fluorescence lifetime imaging of animal feces contaminated apples by time-resolved laser-induced fluorescence imaging system with tunable excitation wavelengths. *Appl. Optics, 47*(10), 1608-1616. http://dx.doi.org/10.1364/AO.47.001608.

Lefcourt, A. M., Kim, M. S., & Chen, Y. R. (2003). Automated detection of fecal contamination of apples by multispectral laser-induced fluorescence imaging. *Appl. Optics, 42*(19), 3935-3943. http://dx.doi.org/10.1364/AO.42.003935.

Lefcourt, A. M., Kim, M. S., & Chen, Y. R. (2005a). Detection of fecal contamination on apples with nanosecond-scaled time-resolved imaging of laser-induced fluorescence. *Appl. Optics, 44*(7), 1160-1170. http://dx.doi.org/10.1364/AO.44.001160.

Lefcourt, A. M., Kim, M. S., & Chen, Y. R. (2005b). Detection of fecal contamination in apple calyx by multispectral laser-induced fluorescence. *Trans. ASAE, 48*(4), 1587-1593. http://dx.doi.org/10.13031/2013.19173.

Lefcourt, A. M., Kim, M. S., & Chen, Y. R. (2005c). A transportable fluorescence imaging system for detecting fecal contaminants. *Computers Electr. Agric., 48*(1), 63-74. http://dx.doi.org/10.1016/j.compag.2005.01.002.

Lefcourt, A., Kim, M. S., Chen, Y. R., & Kang, S. (2006). Systematic approach for using hyperspectral data to develop multispectral imaging systems: Detection of feces on apples. *Computers Electr. Agric., 54*(1), 22-35. http://dx.doi.org/10.1016/j.compag.2006.06.002.

Murata, N., Nishimura, M., & Takamiya, A. (1966). Fluorescence of chlorophyll in photosynthetic systems: III. Emission and action spectra of fluorescence—Three emission bands of chlorophyll *a* and the energy transfer between two pigment systems. *Biochimica et Biophysica Acta (BBA) - Biophysics including Photosynthesis, 126*(2), 234-243. http://dx.doi.org/10.1016/0926-6585(66)90059-8.

Painter, J. A., Hoekstra, R. M., Ayers, T., Tauxe, R. V., Braden, C. R., Angulo, F. J., & Griffin, P. M. (2013). Attribution of foodborne illnesses, hospitalizations, and deaths to food commodities by using outbreak data, United States, 1998-2008. *Emerging Infectious Diseases, 19*(3). http://dx.doi.org/10.3201/eid1903.111866.

Sun, D. W. (2010). *Hyperspectral Imaging for Food Quality Analysis and Control.* London, U.K.: Academic Press.

Tewey, K. (2013). Time-resolved hyperspectral line-scan imaging of pulsed laser-induced fluorescence: Food safety inspection. MS thesis. Baltimore, Md.: University of Maryland, Department of Mechanical Engineering.

Zhang, R., Ying, Y., Raoa, X., & Li, J. (2012). Quality and safety assessment of food and agricultural products by hyperspectral fluorescence imaging. *J. Sci. Food Agric., 92*(12), 2397-2048. http://dx.doi.org/10.1002/jsfa.5702.